



Liquid flow rate control in run-around heat recovery systems

Downloaded from: <https://research.chalmers.se>, 2025-10-22 05:51 UTC

Citation for the original published paper (version of record):

Filipsson, P., Trüschel, A., Lindholm, T. et al (2025). Liquid flow rate control in run-around heat recovery systems. *Science and Technology for the Built Environment*, 31(9): 1077-1090.
<http://dx.doi.org/10.1080/23744731.2025.2538372>

N.B. When citing this work, cite the original published paper.



Liquid flow rate control in run-around heat recovery systems

Peter Filipsson, Jan-Olof Dalenbäck, Anders Trüschel & Torbjörn Lindholm

To cite this article: Peter Filipsson, Jan-Olof Dalenbäck, Anders Trüschel & Torbjörn Lindholm (2025) Liquid flow rate control in run-around heat recovery systems, Science and Technology for the Built Environment, 31:9, 1077-1090, DOI: [10.1080/23744731.2025.2538372](https://doi.org/10.1080/23744731.2025.2538372)

To link to this article: <https://doi.org/10.1080/23744731.2025.2538372>



Copyright © 2025 The Author(s). Published with license by Taylor & Francis Group, LLC.



Published online: 05 Aug 2025.



Submit your article to this journal [↗](#)



Article views: 248



View related articles [↗](#)



View Crossmark data [↗](#)

Liquid flow rate control in run-around heat recovery systems

PETER FILIPSSON^{1,2*} , JAN-OLOF DALENBÄCK¹ , ANDERS TRÜSCHEL¹ , AND TORBJÖRN LINDHOLM¹ 

¹Division of Building Services Engineering, Department of Architecture and Civil Engineering, Chalmers University of Technology, 412 96 Gothenburg, Sweden

²CIT Renergy, Sven Hultins plats 1, 412 58 Gothenburg, Sweden

Run-around heat recovery has been available for over half a century as an option to recover heat in ventilation systems, especially advantageous in buildings with significant space limitations or strict air cleanliness requirements. The core of the system is a liquid transferring heat from the extract air to the supply air. Improper control of the liquid flow rate causes underperformance increasingly as the systems are designed for higher heat transfer effectiveness and more often in combination with demand-controlled ventilation. The work presented in this paper is a combination of experimental measurements and simulations. The results show how much the heat transfer effectiveness can be improved (up to 6% under the studied conditions) by increasing the liquid heat capacity rate from being equal to the heat capacity rate of the air flows, which is the prevalent strategy today. In addition, a novel control method is demonstrated. It is based on measuring temperatures instead of volumetric flow rates, which is the prevalent method today. This method has potential to make the system more robust and accurate, which is key to be able to optimize the liquid flow rate in run-around heat recovery systems in practice.

1. Introduction

To ensure good indoor air quality, commercial buildings generally require large ventilation air flows. To avoid excessive energy use, a heat recovery system can recover heat from the extract air and supply it to the incoming outdoor air. In hot climates, the same system can be used to decrease energy demand for cooling. Rotary heat exchangers and plate heat exchangers are both associated with high thermal performance but also with a risk of internal leakage and require the supply and exhaust air ducts to be located at the same place (Aridi et al. 2021). In contrast, a run-around heat recovery system allows separately located air streams which guarantees no internal leakage and often makes it the only practical option when retrofitting an old ventilation system or when no contamination between exhaust and supply air can be accepted. These advantages are made possible by a coupling liquid which transfers the heat from a fin-and-tube

heat exchanger (coil) in the exhaust air stream to another fin-and-tube heat exchanger in the supply air stream. A principal sketch of such a system is presented in Figure 1. Real systems are often equipped with a three-way-valve for frost protection and capacity control and sometimes also with the possibility to heat or cool the liquid from an external source. The coupling liquid is usually a mixture of water and an antifreeze agent (glycol) and is circulated by a pump. The liquid flow rate has always been an important parameter in run-around heat recovery systems but even more so lately due to designing for better thermal performance (higher heat transfer effectiveness) and more often in combination with demand controlled ventilation air flow rates.

Since the heat recovered by a run-around system must be transferred twice, first in the exhaust air coil and then in the supply air coil, the heat transfer effectiveness is generally lower than in a rotary heat exchanger and in a plate heat exchanger. Typical heat transfer effectiveness of a run-around heat recovery system is 45–65% while corresponding value is 50–80% for plate heat exchangers and >80% for rotary heat exchangers (Mardiana-Idayu and Riffat 2012). According to the European Ecodesign requirements for ventilation units on the EU market, the minimum allowed heat transfer effectiveness of a new run-around heat recovery system is 68% while corresponding value for all other heat recovery systems is 73% (EU 2014). In addition to be inherently low in general, the heat transfer effectiveness of actual run-around heat recovery systems in reality is often worse than designed for, especially in demand-controlled ventilation systems (Mahmoud et al. 2022). Some possible reasons for this are coil fouling (both air and

Received January 9, 2025; accepted July 11, 2025

Peter Filipsson, PhD, is a Researcher. **Jan-Olof Dalenbäck, PhD**, is a Full Professor. **Anders Trüschel, PhD**, is a Senior Lecturer. **Torbjörn Lindholm, PhD**, is a Senior Lecturer.

*Corresponding author e-mail: filipssp@chalmers.se

This is an Open Access article distributed under the terms of the Creative Commons Attribution License (<http://creativecommons.org/licenses/by/4.0/>), which permits unrestricted use, distribution, and reproduction in any medium, provided the original work is properly cited. The terms on which this article has been published allow the posting of the Accepted Manuscript in a repository by the author(s) or with their consent.

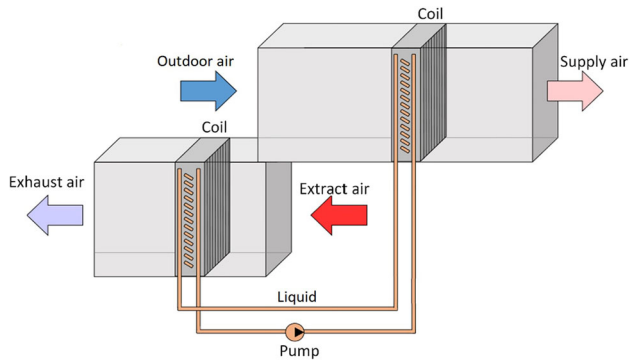


Fig. 1. Principal sketch of a run-around heat recovery system.

liquid side), poor liquid quality, excessive antifreeze agent concentration, malfunctioning valves, improper frost anti-buildup control and unfavorable liquid flow rate. While these are factors that can cause an existing system to underperform, there are several guidelines on how to optimize a new system. These include avoiding laminar flow (both air and liquid side), optimizing the antifreeze agent concentration, designing for low liquid flow rate, using large coil surface area and low pressure drop, optimizing tube wall thickness, optimizing control sequences and using variable speed pumping (Zeng, Besant, and Rezkallah 1992; Bennett et al. 1994; Besant and Johnson 1995; Johnson, Besant, and Schoenau 1995; Nelson 2021). More unconventional ways to improve heat transfer, at the expense of higher pressure drop, are to use nanofluids (Choi and Eastman 1995) and turbulators (Liu and Sakr 2013).

1.1. Liquid flow rate

Most previous studies on the liquid flow rate in run-around heat recovery systems conclude that the heat capacity rate of the liquid should be equal to the heat capacity rate of the air (Balen, Donjerković, and Galaso 2003; Emerson 1984; Holmberg 1975; Kays and London 1984; London and Kays 1951), since that implies optimum temperature differences in the coils. Wallin, Madani, and Claesson (2009) on the other hand, discerned how the liquid flow rate influences the overall heat transfer coefficient. A similar technology, which additionally enables moisture recovery, is run-around membrane energy exchanger. Rasouli et al. (2011) investigated optimization of these systems and showed that the optimum liquid flow rate depends on the outdoor air conditions. In heating mode, the optimum heat capacity rate of the liquid was shown to be slightly higher than that of the air, whereas in cooling mode, it was shown to be significantly (around three times) higher. Mahmoud et al. (2022) combined the knowledge of optimum temperature difference with the fact that higher flow rate implies higher convective heat transfer coefficient. Consequently, it was concluded that the liquid flow rate should be slightly higher than traditionally suggested, also for pure sensible run-around heat recovery. Up to a certain liquid flow rate, the profit of better heat transfer coefficients outweighs the loss of worsened temperature difference. At this certain liquid flow rate, the heat transfer effectiveness is at its maximum. The present paper adds to this research by

investigating how the results depends on the air flow rate, which is especially important with demand-controlled ventilation, and presents a novel method to control it.

1.2. Liquid flow rate control

Detailed knowledge about optimum liquid flow rate is of limited value if there is no reliable method to control it. Therefore, the present paper also presents an unconventional and robust method to control the liquid flow rate in run-around heat recovery systems.

Conventional methods to control the liquid flow rate in run-around heat recovery systems involves measuring the liquid flow rate (AL-KO 2024; FläktGroup 2024; Trox 2024; Robatherm 2024), in order to match it with the air flow rates. These methods require knowledge about the mass flow rates of the air flows (usually determined by measuring the volumetric flow rates), the specific heat capacities of the air, the mass flow rate of the liquid (usually determined by measuring the volumetric flow rate) and the specific heat capacity of the liquid. All of these parameters are associated with varying degrees of uncertainty. One common method to determine the volumetric flow rate of the liquid is measuring the pressure drop across one of the coils or across an orifice plate. Unfortunately, the glycol concentration and temperature affect the thermophysical properties of the liquid in a way that makes the system very sensitive to uncertainties. Adding glycol (or decreasing the temperature) decreases the specific heat capacity while increasing the viscosity, see Figure 2. As a result, the required liquid flow rate is increased while (if not taken into account by the flow rate measurement) the actual liquid flow rate is decreased (since the pressure drop sensor interpret the higher pressure drop as a higher flow rate). The influence of viscosity on pressure drop is especially obvious for laminar flow but also true for turbulent flow.

Relevant thermophysical properties of common used liquids are presented in Figure 2. Please note that the y-axes' max-min ratios of the specific heat, density and conductivity are equal, to facilitate a comparison of how much they are influenced by the glycol concentration. The dynamic viscosity however, is influenced to an extent beyond that comparison. Even the least influenced liquid, ethylene glycol at 20 °C, has a 35% increase in dynamic viscosity when the concentration is increased from 30% to 40%. In cold climates, ethylene glycol is often preferred due to its comparatively low dynamic viscosity at low temperatures. In warm climates, propylene glycol is often preferred due to its nontoxicity (Nelson 2021). The influence of temperature on the thermophysical properties is relevant since the same heat recovery system can supply a major part of the total cooling demand during summer (Filipsson et al. 2020).

The freezing point as a function of glycol concentration is presented in Figure 3. It shall be noted that some guidelines recommend using the lowest concentration of glycol possible based on burst temperature instead (Nelson 2021) (which is significantly lower than the freezing point), while other state that the burst temperature is relevant only for systems that are dormant or inactive at temperatures below the

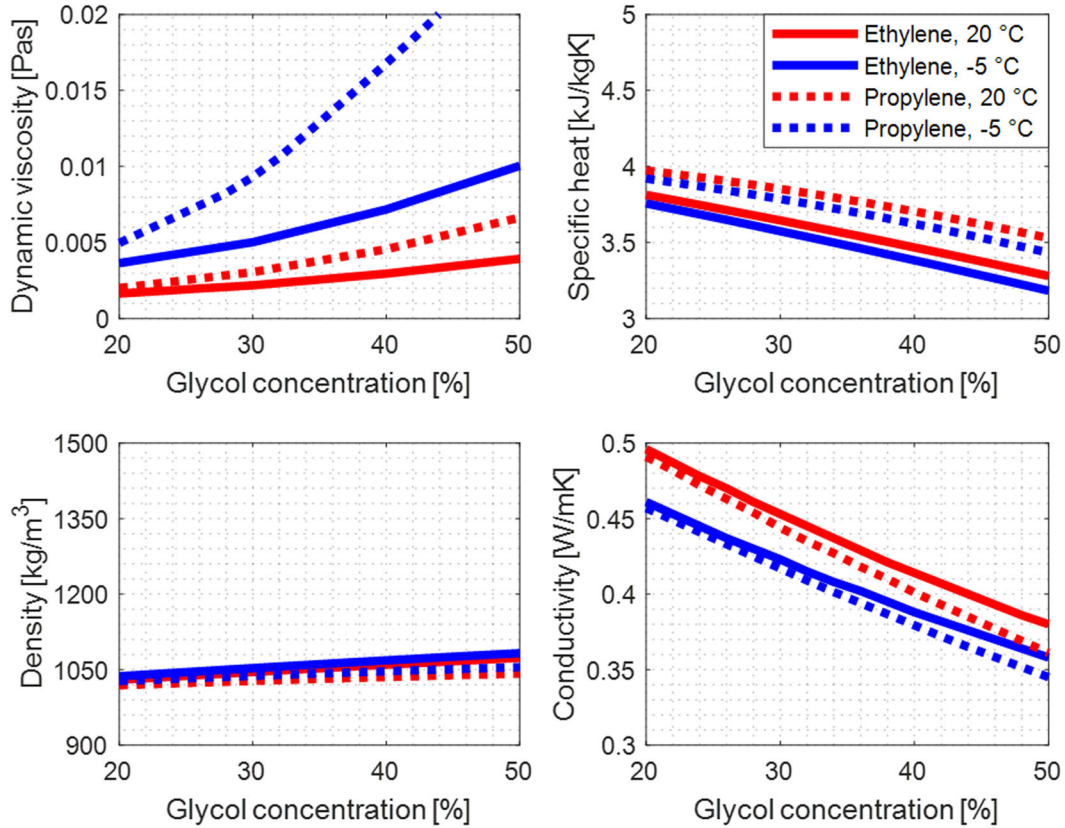


Fig. 2. Dynamic viscosity, specific heat, density and conductivity of ethylene glycol and propylene glycol at two different temperatures as a function of glycol concentration (Jacobsen, Rasmussen and Andersen 1999).

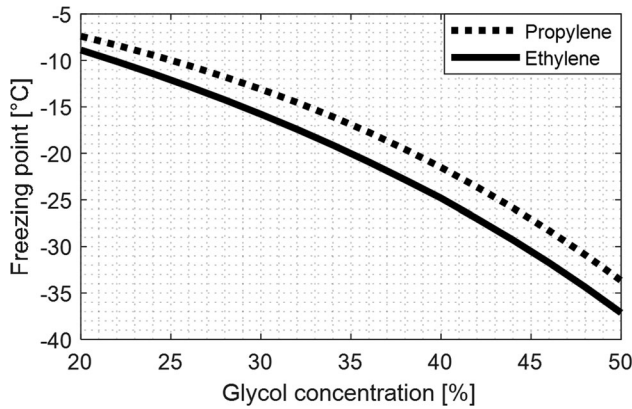


Fig. 3. Freezing point of propylene glycol and ethylene glycol as a function of glycol concentration (Jacobsen, Rasmussen and Andersen 1999).

freezing point (Janssen 2016), since slush creation during operation is undesirable.

As pointed out in many previous studies, glycol is detrimental to the thermal performance of run-around heat recovery systems (Mahmoud et al. 2022; Nelson 2021). An old rule of thumb is that the heat transfer effectiveness is decreased by 1% by every 10% increase in glycol concentration (Holmberg and Strindehag 1981). However, this rule of thumb presupposes

that the liquid flow rate is as desired also after the increased glycol concentration, which requires the control system to be aware of the increase. One potential method to ensure that would be to monitor the thermophysical properties of the liquid (or at least glycol concentration and temperature) in order for the control system to take it into account. However, the flow rate of the liquid is by no means relevant per se, what is important is its temperature. Therefore, an unconventional control method based on temperatures is proposed in this article. A similar approach was presented by Emerson (1984), who stated that the maximum rate of heat recovery was achieved when the upper terminal temperature difference of the exhaust air coil divided by the upper terminal temperature difference of the supply air coil is equal to the lower terminal temperature difference of the exhaust air coil divided by the lower terminal temperature difference of the supply air coil. Or in other words, when Eq. (1) holds true.

$$\frac{t_{ea} - t_{l,w}}{t_{l,w} - t_{sa}} = \frac{t_{eha} - t_{l,c}}{t_{l,c} - t_{oa}} \quad (1)$$

t_{ea} , t_{sa} , t_{eha} , t_{oa} , $t_{l,w}$ and $t_{l,c}$ are the temperatures of extract air, supply air, exhaust air, outdoor air, warm liquid and cool liquid respectively. The present paper adds to this research partly by adjusting it with regards to the findings of Mahmoud et al. (2022) and partly by validating the method with actual data, both from simulations and measurements.

2. Material and methods

This section is divided into three parts, a description of the model used for simulations, a presentation of the experimental setup used for measurements and finally the theory behind the proposed control method.

2.1. Model description

The model used for simulations in this paper is based on the model presented by Mahmoud et al. (2022), which in turn is based on the model presented by Holmberg (1975). The model is represented by Eqs (2)–(15), and all calculations were carried out in the numerical computing software MATLAB R2022b (MathWorks 2022).

The overall heat transfer effectiveness of the run-around heat recovery system is defined as the ratio between the actual heat recovered and the theoretical maximum, see Eq. (2).

$$\varepsilon_O = \frac{q}{q_{\max}} \quad (2)$$

The overall heat transfer effectiveness is determined by Eq. (3), where ε_c and ε_w are the effectiveness of the supply and exhaust air coils, respectively. C_l is the liquid heat capacity rate, $C_{\min,o}$ is the minimum heat capacity rate of the two air flows while $C_{\min,c}$ and $C_{\min,w}$ are the minimum heat capacity rates of the air and the liquid in the supply and exhaust air coils, respectively.

$$\varepsilon_O = \frac{1}{\frac{C_{\min,o}/C_{\min,w}}{\varepsilon_w} + \frac{C_{\min,o}/C_{\min,c}}{\varepsilon_c} - \frac{C_{\min,o}}{C_l}} \quad (3)$$

Heat capacity rates are calculated as the product of volumetric flow rate, density and specific heat capacity, according to Eq. (4).

$$C = \dot{V} \cdot \rho \cdot c_p \quad (4)$$

The heat transfer effectiveness of each coil is determined according to Eq. (5), where C_r is the ratio between the smaller and larger heat capacity rate passing through the coil.

$$\varepsilon = \frac{1 - e^{NTU \cdot (C_r - 1)}}{1 - C_r \cdot e^{NTU \cdot (C_r - 1)}} \quad (5)$$

The number of transfer units, NTU , is determined by Eq. (6), while the product of overall heat transfer coefficient and area, UA , is calculated by Eq. (7).

$$NTU = \frac{UA}{C_{\min}} \quad (6)$$

$$UA = \frac{1}{\frac{1}{h_l A_l} + \frac{\ln(d_o/d_i)}{2\pi k_l L} + \frac{1}{(hA)_a}} \quad (7)$$

The three terms in the right-hand side denominator of Eq. (7) represent the heat transfer resistances of the liquid side, the tubes and the air side, respectively. d_o and d_i are the outside and inside tube diameter, L is the total tube length and k_l is the thermal conductivity of the tube material. A_l is the

liquid side heat transfer area while the convective heat transfer coefficient, h_l , is determined by Eq. (8).

$$h_l = \frac{Nu \cdot k_l}{d_i} \quad (8)$$

k_l is the thermal conductivity of the liquid and the Nusselt number, Nu , is calculated according to Gnielinski's empirical correlation (Eq. (9)) when the Reynolds number is above 2300.

$$Nu = \frac{(f/8) \cdot (Re - 1000) \cdot Pr}{1 + 12.7 \cdot \sqrt{f/8} \cdot (Pr^{2/3} - 1)} \quad (9)$$

Pr is the Prandtl number, and f is the Fanning friction factor determined by Eq. (10).

$$f = (0.79 \cdot \ln(Re) - 1.64)^{-2} \quad (10)$$

For Reynolds numbers below 2300, the Nusselt number is determined according to Eqs. (11)–(14), where l is the straight length of one tube (Ghiassian 2018).

$$Nu = (Nu_1^3 + 0.6^3 + (Nu_2 - 0.6)^3 + Nu_3^3)^{1/3} \quad (11)$$

$$Nu_1 = 4.364 \quad (12)$$

$$Nu_2 = 1.953 \cdot \left(\frac{d_i}{l}\right)^{1/3} \cdot (Re \cdot Pr)^{1/3} \quad (13)$$

$$Nu_3 = 0.924 \cdot Pr^{1/3} \cdot \sqrt{\frac{d_i \cdot Re}{l}} \quad (14)$$

In contrast to the model presented by Mahmoud et al. (2022), the complex air side geometry is now lumped into two characteristic parameters X and Y . This means that the air side convective heat transfer is represented by a grey box model, according to Eq. (15). This approach was originally presented by Rabehl, Mitchell, and Beckman (1999) and previously adopted by Filipsson et al. (2017).

$$(hA)_a = X \cdot k_a \left(\frac{\dot{V}_a \rho_a}{\mu_a}\right)^Y \cdot Pr_a^{0.36} \cdot \left(\frac{Pr_a}{Pr_{as}}\right)^{0.25} \quad (15)$$

X and Y are determined by minimizing the root mean square error between simulated and measured overall heat transfer effectiveness. k_a is the thermal conductivity of the air, μ_a is the dynamic viscosity of the air and Pr_{as} is the Prandtl number of the air evaluated at the tube surface temperature. All fluid properties, except Pr_{as} , are evaluated at the arithmetic mean value of the inlet and outlet temperature of each fluid in each heat exchanger. The source of all fluid properties is the simulation tool CoolPack (Jacobsen, Rasmussen, and Andersen 1999).

As said, the overall heat transfer effectiveness is determined by Eqs. (3)–(15). With equal flow rates of supply and exhaust air and no occurrence of condensation, the overall heat transfer effectiveness (Eqs. (2) and (3)) is also equal to Eq. (16). Eq. (16) represents how the overall heat transfer effectiveness was determined by measurements.

$$\varepsilon_O = \frac{t_{sa} - t_{oa}}{t_{ea} - t_{oa}} \quad (16)$$

Henceforth, the overall heat transfer effectiveness is referred to simply as heat transfer effectiveness.

2.2. Experimental setup

The run-around heat recovery system used for experiments in this study is schematically presented in Figure 4. Resistance temperature detector (RTD) sensors are located in the outdoor air, supply air, extract air, exhaust air, the cool liquid side and up- and downstream of the pump on the warm liquid side. The liquid flow rate was determined with an IMI TA STAD-PN 25 balancing valve with an uncertainty of 5% and an IMI TA-SCOPE pressure drop sensor with an uncertainty of 1%. Air flow rates were measured with fan integrated differential pressure sensors. Accordance of the air flow sensors was ensured by short-circuiting the supply and extract air while checking that the sensors measured equal air flow rates. All RTD sensors were calibrated against a Dostmann P650 temperature sensor with an uncertainty of $\pm 0.02^\circ\text{C}$. Temperature distributions across the cross-section of the air flows were measured and taken into account. This was measured by four temperature sensors, each in the center of a quadrant of the cross-section. Between the coils and the fans, the maximum difference between these four sensors were 0.4°C which led to the conclusion that four measurement points were sufficient. Influence of fan heat dissipation were also measured and taken into account. Hence, temperatures presented in this study corresponds to the average temperature across the cross-section and the exhaust and supply air temperatures represents the temperature upstream the fans (in contrast to the location of the sensors). The main reason to locate the sensors downstream of the fans is to obtain conditions closer to fully mixed. The rationale for having only one sensor on the cool side of liquid circuit is that this pipe is short and well insulated. Hence, it is assumed that the liquid outlet temperature of the supply air coil equals the liquid inlet temperature of the exhaust air coil.

The experiments were carried out with water as the liquid transferring heat from the extract to the supply air. In contrast to many real applications, no glycol was used in the experiments. The exhaust air flow was always equal to the supply

air flow. Four air flow rates were tested: 250 l/s, 500 l/s, 750 l/s and 1000 l/s. Nonoccurrence of condensation was ensured by almost pure sensible heat gain between supply and extract air (a sensible heat ratio of around 97.5% in the worst case). Outdoor air temperature was $2.1\text{--}5.4^\circ\text{C}$, extract air temperature was $18.9\text{--}21.0^\circ\text{C}$ and liquid flow rate $0.03\text{--}0.53\text{ l/s}$. A total of 82 sets of stable steady-state conditions were tested. These are all declared in the Appendix. A photograph of the experimental setup is presented in Figure 5. The air streams are arranged as in the schematic drawing, the pump is not included in the photograph and the pipework was insulated during the measurements.

2.3. Control method

As pointed out in section 1.2, the prevalent method of controlling the liquid flow rate requires knowledge about the air flow rates, the thermophysical properties of the fluids (air and liquid) and the regime and a pressure drop of the liquid flow. Thenceforth, the pump speed is controlled to satisfy Eq. (17).

$$\dot{V}_l = \frac{\dot{V}_a \cdot \rho_a \cdot c_{p,a}}{\rho_l \cdot c_{p,l}} \quad (17)$$

Fulfillment of Eq. (17) is called balanced heat capacity rates and also a heat capacity ratio of one. The heat capacity ratio is defined as Eq. (18).

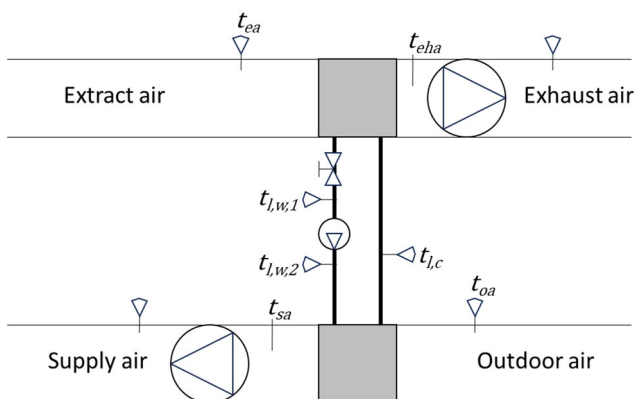


Fig. 4. Schematic drawing of the experimental setup.

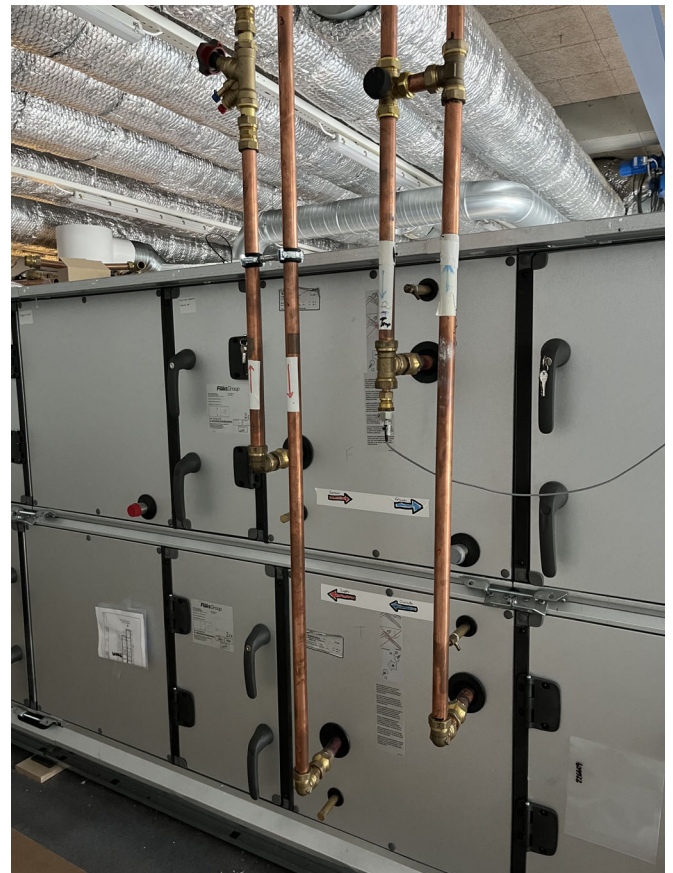


Fig. 5. Photograph of the experimental setup.

$$x_V = \frac{\dot{V}_l \cdot \rho_l \cdot c_{p,l}}{\dot{V}_a \cdot \rho_a \cdot c_{p,a}} \quad (18)$$

A heat balance over the supply air coil can be written as Eq. (19).

$$\dot{V}_a \cdot \rho_a \cdot c_{p,a} \cdot (t_{sa} - t_{oa}) = \dot{V}_l \cdot \rho_l \cdot c_{p,l} \cdot (t_{l,w,2} - t_{l,c}) \quad (19)$$

By combining Eq. (18) and Eq. (19), the heat capacity ratio may be expressed as Eq. (20),

$$x_{t,1} = \frac{t_{sa} - t_{oa}}{t_{l,w,2} - t_{l,c}} \quad (20)$$

x_V equals $x_{t,1}$ by definition, but the subscripts reveal the method of how it is determined. Using Eq. (20) to determine the ratio requires no information about either flows or thermophysical properties, neither for air nor for liquid.

3. Results

This section is divided into model validation, simulations and control method. Model validation is a comparison of simulations with experiments, the simulation part implies using the model to explore conditions that were not tested in the experiments and the control method part quantifies the disadvantage of the conventional control method and shows the potential of the suggested control method.

3.1. Model validation

Figure 6 shows heat transfer effectiveness, measured and simulated, as a function of liquid (water) flow rate at four different air flow rates.

It can be noted that the peak heat transfer effectiveness is rather unaffected by the air flow rate. On the one hand, higher flow rates (of air and liquid) generates higher

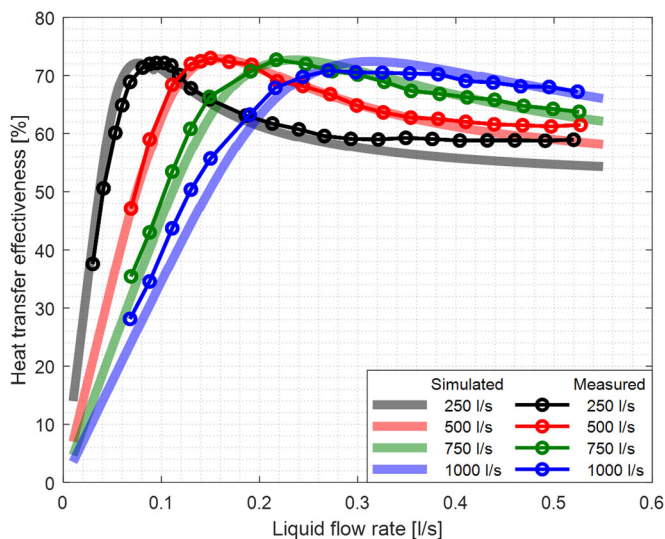


Fig. 6. Measured and simulated heat transfer effectiveness as a function of liquid (water) flow rate at four different air flow rates.

convective heat transfer coefficients. On the other hand, the higher volumetric flow rates means higher heat capacity rates and thus relatively smaller heat exchangers (lower NTU). The results indicate that the influence of these two phenomena are of similar magnitude. It can also be noted that the model underestimates the heat transfer effectiveness at high liquid flow rates, especially at low air flow rates. This indicates that the liquid flow rates' influence on convective heat transfer is somewhat higher than suggested by the model.

3.2. Simulations

In practice, an antifreeze agent is usually added to the liquid in order to avoid freezing during sub-zero conditions. Figure 7 shows the simulated heat transfer effectiveness as a function of liquid flow rate at four different air flow rates, both with water and with 30% ethylene glycol.

From Figure 7, it can be noted that the ethylene glycol reduces the peak heat transfer effectiveness (due to lower thermal conductivity and higher viscosity), the peak is also shifted toward higher volumetric liquid flow rates (due to lower specific heat capacity) and the transition between laminar and turbulent flow becomes more noticeable and occurs at higher liquid flow rates (due to higher viscosity).

In Figure 8, the heat transfer effectiveness is plotted against the liquid (30% ethylene glycol) flow rate at an air flow rate of 750 l/s. The vertical lines represent liquid flow rates corresponding to balanced heat capacity rates and maximum heat transfer effectiveness respectively. Balanced heat capacity rates means that the average heat capacity rate of the liquid is equal to the average heat capacity rates of the air flows (a heat capacity ratio equal to one). The term *average* is meaningful since density and specific heat capacity depends on temperature. Hence, equal volumetric flow rates

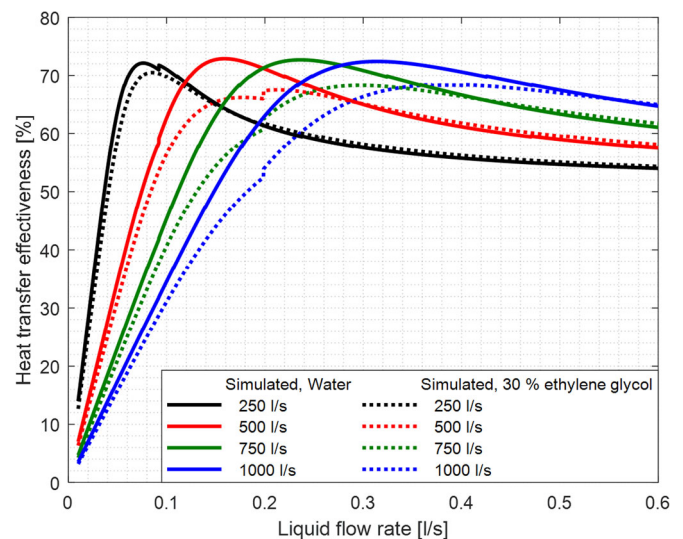


Fig. 7. Heat transfer effectiveness with pure water and with 30% ethylene glycol, as a function of liquid flow rate at four different air flow rates.

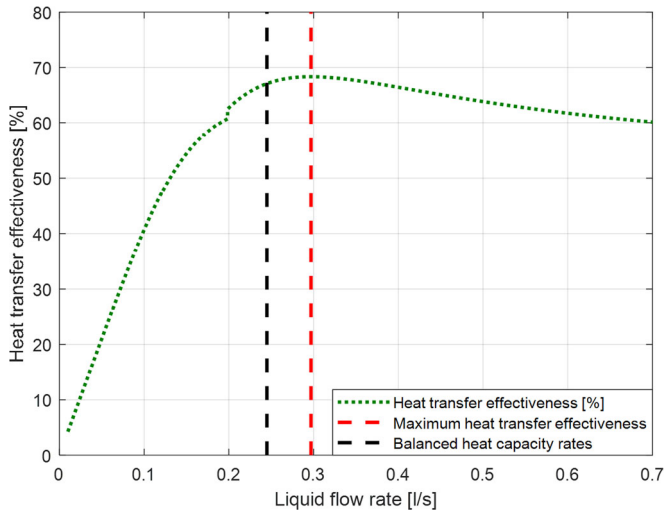


Fig. 8. Heat transfer effectiveness as a function of liquid flow rate at air flow rate of 750 l/s and 30% ethylene glycol.

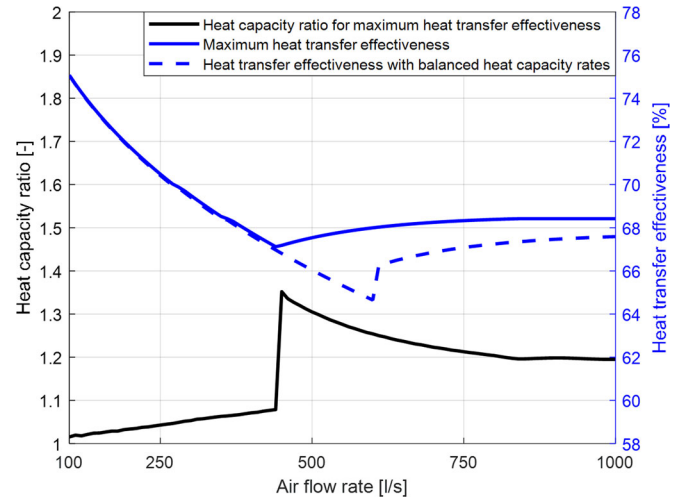


Fig. 10. Heat transfer effectiveness and heat capacity ratio for maximum heat transfer effectiveness as a function of air flow rate (30% ethylene glycol).

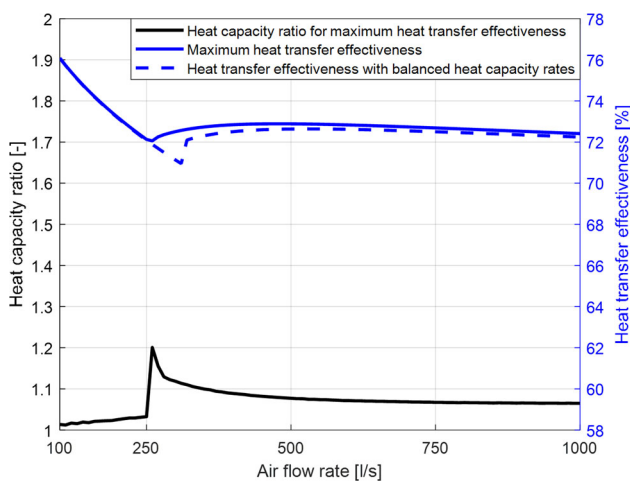


Fig. 9. Heat transfer effectiveness and heat capacity ratio for maximum heat transfer effectiveness as a function of air flow rate (0% ethylene glycol).

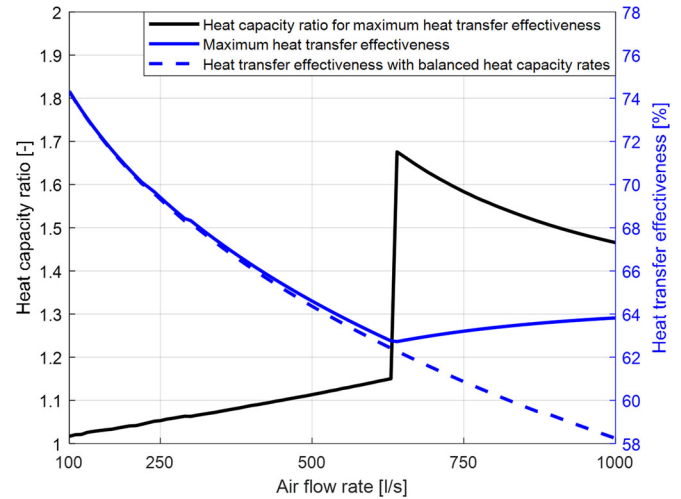


Fig. 11. Heat transfer effectiveness and heat capacity ratio for maximum heat transfer effectiveness as a function of air flow rate (50% ethylene glycol).

of supply and exhaust air implies unequal heat capacity rates.

Figure 8 reveals that the flow rate generating the maximum heat transfer effectiveness is 21% higher than the liquid flow rate corresponding to balanced heat capacity rates. This ratio is henceforth referred to as heat capacity ratio for maximum heat transfer effectiveness. In Figure 9, the heat capacity ratio for maximum heat transfer effectiveness is plotted as a function of air flow rate. In addition, the heat transfer effectiveness of the two liquid flow rates are also presented.

The behavior of the effectiveness in the figure can be explained by dividing the air flow rate interval into three modes. At below 250 l/s, the liquid flow is laminar both at balanced capacity rate and at maximum effectiveness. At 250–310 l/s, it is laminar at balanced capacity rate and turbulent at maximum heat transfer effectiveness and at above

310 l/s it is turbulent at both. While Figure 9 refers to pure water as the heat transferring liquid, Figure 10 shows the results corresponding to 30% ethylene glycol.

As seen in Figure 10, the difference between balanced heat capacity rates and maximum heat transfer effectiveness flow is larger, both regarding heat capacity rates and the benefit from a higher heat transfer effectiveness. The difference is further increased with a higher ethylene glycol concentration, see Figure 11, which corresponds to 50% ethylene glycol.

3.3. Control method

With the model at hands, it is possible to quantify the consequence of erroneously assumed glycol concentration (described in Section 1.2). Assume the ethylene glycol concentration in a run-around heat recovery system is increased

from 30% to 50%, without taken into account by the control system. The negative consequence is tripartite:

- Reduced heat transfer coefficient due to lower conductivity and higher viscosity.
- Higher required liquid flow rate due to reduced specific heat capacity.
- Lower actual liquid flow rate due to reduced pump speed due to higher pressure drop due to increased viscosity.

While the first one is an inevitable drawback of increased glycol concentration, the two other may be compensated for or avoided by a proper control system. The second one is to some extent mitigated by the fact that the density is increased when the glycol concentration is increased, provided that the control system measures volumetric flow rate (not mass flow rate). The magnitude of the third one also depends on how the liquid flow rate is determined. In this example, the liquid flow rate is determined by measuring a pressure drop which is assumed to be proportional to the dynamic viscosity of the liquid. The continuous lines in Figure 12 shows the heat transfer effectiveness as a function of the liquid flow rate at two different air flow rates. The yellow and green markers represent the flows of balanced heat capacity rates and the maximum heat transfer effectiveness, which were the focus of the previous section of this paper. The dotted lines represent a scenario where the ethylene glycol concentration is increased to 50%.

As seen in Figure 12, the liquid flow rate needs to be increased, when increasing the glycol concentration, in order to balance the heat capacity rates. If not, a slightly lower heat transfer effectiveness is obtained (grey markers). However, the major spoilage of the heat transfer effectiveness appears if the control system do not take into account the higher viscosity of the liquid and reduces the pump speed accordingly, see the red markers. Yellow and green markers correspond to the heat transfer effectiveness and capacity ratios in Figures 10 and 11.

While the purpose of Figure 12 is to quantify a drawback of conventional control systems, the purpose of Figure 13 is to demonstrate the possibility to control the systems with respect to temperatures. Figure 13 shows simulated data

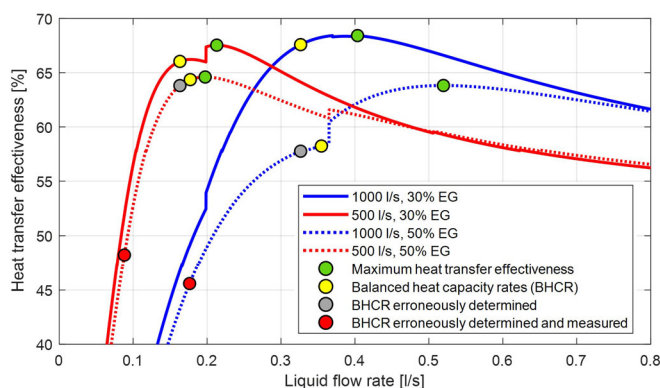


Fig. 12. Heat transfer effectiveness for 1000 and 500 l/s and at 30 and 50% ethylene glycol (EG) concentration.

with 30% ethylene glycol and at an air flow rate of 750 l/s. The vertical lines in Figure 13(a) represents the flow rates in Figure 13(b–d).

Figure 14 compares the heat transfer effectiveness as a function of the heat capacity ratio determined by flow rate measurements (Eq. (18)) and by temperature measurements (Eq. (20)).

Since pure water was used in the measurements, Figure 14 should correspond to the simulations in Figure 9. A higher glycol concentration would result in a more clear shift of the peaks toward higher heat capacity ratio. Although the proposed control method has not been tested dynamically in this work, Figure 14(b) can be seen as an encouraging proof of concept.

3.4. Uncertainty analysis

Determination of the heat transfer effectiveness involves measuring the temperatures of the outdoor air, the extract air and the supply air. As previously stated, the sensors were calibrated against a high precision thermometer (Dostmann P650) with a declared uncertainty of $\pm 0.02^\circ\text{C}$. Therefore, the total measurement uncertainty is instead dominated by the heterogeneous temperature profile across the cross-section of the supply airflow. As previously mentioned, the supply air temperature was measured at four positions in the center of each quadrant across the cross-section and the maximum difference between the highest and lowest was 0.4°C . Disregarding the fact that this sample is not random, a statistical analysis can be applied where four samples are extracted from a population of which the mean value is of interest. The mean value and the standard deviation of the sample yielded that the population mean is within $\pm 0.33^\circ\text{C}$ of the sample mean (at a 95% confidence level). For the resulting heat transfer effectiveness, this represents ± 2 percentage points. However, this is a worst-case analysis, since 0.4°C was the maximum range, and also because the sensors were positioned in a way that would make the sample mean as close as possible to the population mean, in contrast to a random sample.

Assuming adiabatic conditions, the heat transferred to the supply air equals the heat transferred from the exhaust air plus the heat dissipated from the pump to the liquid. The deviation from this heat balance is presented (as heat imbalance) in the appendix. The average heat imbalance of all 82 sets of experiments is 1.2%. The average absolute heat imbalance is 4.0%. The maximum heat imbalance (23.7%) appeared at the combination of maximum air flow and minimum liquid flow. At those conditions, the liquid undergoes a rapid change of temperature when entering the coil. This indicates that accurate measurements at these rare conditions require more temperature sensors across the cross-section of the air flow.

4. Discussion

It was shown (in Figure 11) that the heat transfer effectiveness at 1000 l/s could be increased from 58% to 64% by

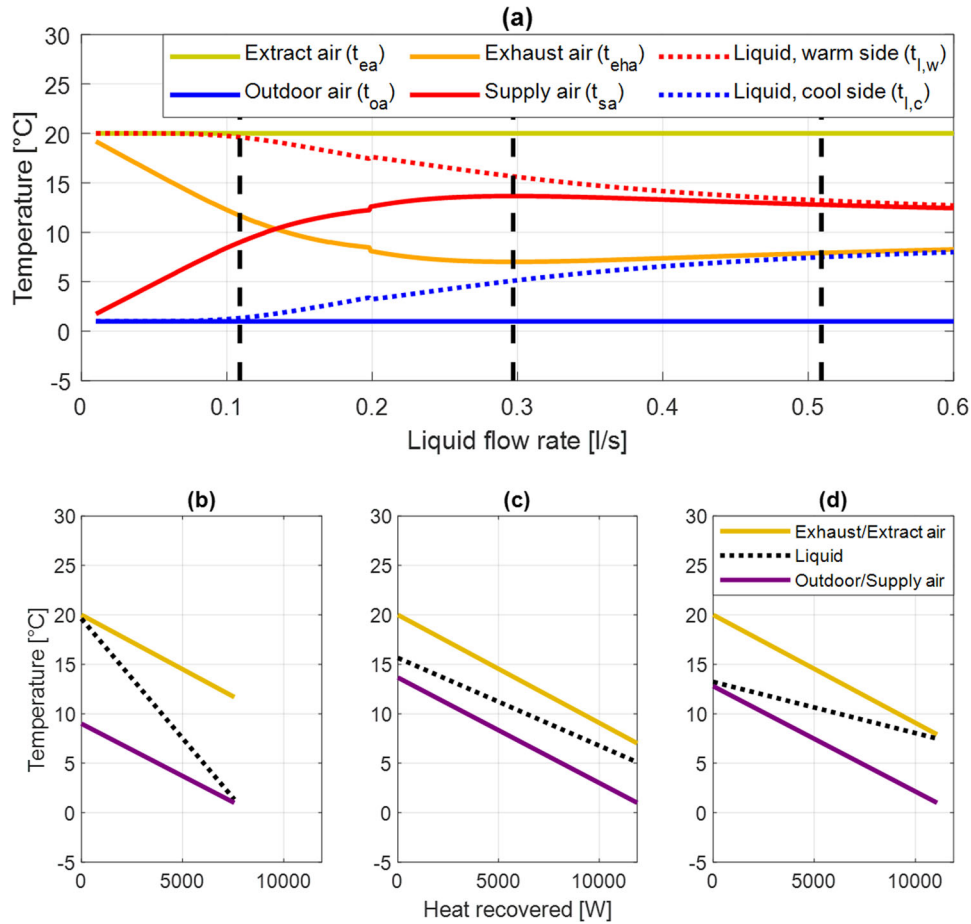


Fig. 13. Temperatures as a function of liquid flow rate (a) and temperatures and heat recovered at too low flow rate (b) at flow rate corresponding to maximum heat transfer effectiveness (c) and at too high flow rate (d).

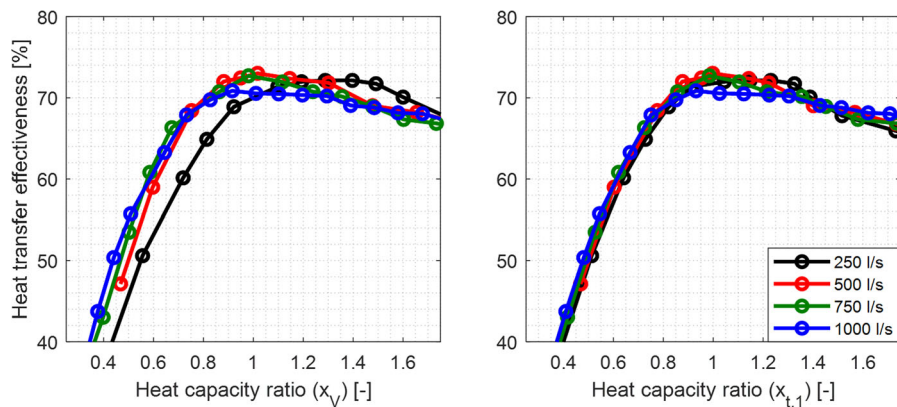


Fig. 14. Heat transfer effectiveness as a function of heat capacity flow ratio based on measurements of the flow rates (a) and based on temperatures (b).

optimizing the liquid flow. For an air handling unit in a climate representing Stockholm in Sweden, with supply and exhaust air temperatures of 20 and 22 °C respectively, this corresponds to an energy saving of 4.3 MWh per year. It was also shown (in Figure 12) that the proposed control method at 1000 l/s could increase the heat transfer effectiveness from 46% to 64%. Using the same conditions as above, this corresponds to an energy saving of 13.0 MWh per year.

It was shown that it is enough to involve the temperatures of one of the coils in the novel control method (Eq. (20)). This is true only if the two air flow rates are equal, otherwise the air inlet and outlet temperatures of both coils need to be measured. In that case, Eq. (20) may be replaced by Eq. (20), where $x_{t,2}$ represents the average ratio of the two coils. While Eq. (20) is a fair compromise, further research is required to conclude whether it is optimal.

$$x_{i,2} = \frac{t_{ea} - t_{eha} + t_{sa} - t_{oa}}{t_{l,w,1} + t_{l,w,2} - 2 \cdot t_{l,c}} \quad (21)$$

Another advantage of measuring the temperatures of both coils is that it is possible to detect performance deterioration since, e.g. fouling of one of the coils will cause the average liquid temperature to be closer to the air temperature of the cleaner coil. A third advantage of measuring inlet and outlet temperatures of both coils is that it reveals any undesired air flow imbalances. This third advantage is not restricted to run-around heat recovery systems, but is valid in any heat recovery system given that no air leakage or condensation occur.

Another advantage of the proposed control method is that it also can handle latent heat transfer. When latent heat is transferred, e.g. by condensation on the exhaust air coil, optimum liquid flow rate is higher than if only sensible heat is transferred. This is taken into account by the proposed control method but not by the conventional one.

In this study, propagation of measurement uncertainties of the suggested control method was not analyzed. It shall be noted that the error caused by uncertainties is smaller when there is a larger difference between exhaust and outdoor temperatures. I.e. the proposed method works as best when it is most needed (when it is cold outside).

In this study, electricity required to run the circulation pump was not taken into account. With this taken into account, the optimum liquid flow rate is lower than that corresponding to maximum heat transfer effectiveness. The size of the deviation depends on the pump efficiency, the pipe pressure drop and the prices of electricity and heat.

When the drawback of the conventional control method was quantified, the ethylene glycol concentration was increased from 30% to 50%. Even though inadequate glycol concentration may occur in systems with unclear liquid quality guidelines, this scenario may seem far stretched. On the other hand, in reality there are many other factors causing a mismatch between actual and anticipated thermophysical properties. Some examples are aging, degradation, oxidation, contamination, temperature and refilling of wrong type of glycol. All of which discourages the conventional control method but do not affect the proposed one.

In this study, the conventional control method was represented by determining the liquid flow rate by measuring a pressure drop. Many other liquid flow meter methods exist, such as electromagnetic, ultrasonic, thermal, rotameter etc. with varying uncertainties and requirements of knowing the liquid properties.

It shall be noted that the model in this study assumed full transition from laminar to turbulent flow at a Reynolds number of 2300. Since the reality is not that distinct, lines representing capacity ratios and heat transfer effectiveness in Figures 9–11 would be smoother if based on measurements.

The results presented in this article can be implemented both in new and existing systems. It thereby facilitates and improves the use of flexible heat recovery with no internal leakage, which are inherent and increasingly valuable features of run-around heat recovery.

In practice, the proposed control method involves adjusting the pump speed to achieve the desired heat capacity ratio (Eq. (20)). Future research is to implement and test the proposed control method in a real run-around heat recovery system. Such test can help finding suitable control parameters. Since the proposed control method is a feedback-control, finding control parameters is a tradeoff between speed and stability. Achieving satisfactory control may require control parameters changing with respect to the air flow rate. Another suggestion for future research is to control the liquid flow rate based on measured heat transfer effectiveness, which would have both advantages and disadvantages compared to the method proposed in the present paper. Future research may also investigate how the temperature influence the heat capacity ratio for maximum heat transfer effectiveness.

4.1. Conclusions

By simulations supported by measurements, this paper shows how much the heat transfer effectiveness of a run-around heat recovery system can be improved by operating at a liquid flow rate different from balanced heat capacity rates (up to 3% with 30% ethylene glycol and up to 6% with 50% ethylene glycol, under the investigated conditions). It is also shown how much higher this liquid flow rate is compared to balanced heat capacity rates. This novel information has a sole academic value if there are no practical and accurate method to control the liquid flow rate. Hence, a novel control method is proposed and explained. The main benefits of the proposed control method is that it requires no information about the thermophysical properties of the liquid and is thereby more robust and more likely to avoid faulty operation. It was shown that the heat transfer effectiveness decreases from around 68% to around 46% if a conventional control system is set to 30% ethylene glycol concentration while it is actually 50%.

Nomenclature

A	= Area [m ²]
C	= Heat capacity rate [W/K]
c_p	= Specific heat capacity [J/kgK]
d	= Diameter [m]
ε	= Heat transfer effectiveness [-]
f	= Fanning friction factor [-]
h	= Convective heat transfer coefficient [W/m ² K]
k	= Thermal conductivity [W/mK]
L	= Length [m]
μ	= Dynamic viscosity [Pas]
NTU	= Number of transfer units [-]
Nu	= Nusselt number [-]
Pr	= Prandtl number [-]
q	= Heatflow [W]
ρ	= Density [kg/m ³]
Re	= Reynolds number [-]
t	= Temperature [°C]
U	= Overall heat transfer coefficient [W/m ² K]

\dot{V} = Volumetric flow rate [m³/s]
 x = Heat capacity ratio [-]
 X, Y = Characteristic parameters [-]

Subscripts

a = air
 as = air at surface
 c = cool
 ea = extract air
 eha = exhaust air
 i = inside
 l = liquid, length
max = maximum
min = minimum
 o = overall, outside
 oa = outdoor air
 r = ratio
 sa = supply air
 t = tube, thermal
 V = volumetric
 w = warm

Acknowledgements

The authors would like to thank Håkan Larsson for technical support and FläktGroup for providing experimental equipment.

Disclosure statement

No potential conflict of interest was reported by the author(s).

Funding

This study was funded by the Swedish Energy Agency (project P2018-90129).

ORCID

Peter Filipsson  <http://orcid.org/0000-0002-2385-0951>
Jan-Olof Dalenbäck  <http://orcid.org/0000-0001-8771-0416>
Anders Trüschel  <http://orcid.org/0000-0002-2951-8378>
Torbjörn Lindholm  <http://orcid.org/0000-0002-4001-8438>

References

- AL-KO Run-around-coil Systems 2024. <https://alko-airtechnology.com/en/wp-content/uploads/sites/4/2022/03/Run-around-coil-systems%E2%80%9393Brochure-EN.pdf>
- Aridi, R., J. Faraj, S. Ali, M. Gad El-Rab, T. Lemenand, and M. Khaled. 2021. Energy recovery in air conditioning systems: Comprehensive review, classifications, critical analysis, and potential recommendations. *Energies* 14 (18):5869. DOI: [10.3390/en14185869](https://doi.org/10.3390/en14185869).
- Balen, I., P. Donjerković, and I. Galaso. 2003. Analysis of the coil energy recovery loop system. *International Journal of Energy Research* 27 (4):363–76. DOI: [10.1002/er.881](https://doi.org/10.1002/er.881).
- Bennett, I. J. D., R. W. Besant, G. J. Schoenau, and A. B. Johnson. 1994. A procedure for optimizing coils in a run-around heat exchanger system. *ASHRAE Trans* 100 (1):230–7.
- Besant, R. W., and A. B. Johnson. 1995. Reducing energy costs using run-around systems. *ASHRAE Journal* 37 (2):41–6.
- Choi, S. U. S., and J. A. Eastman. 1995. Enhancing thermal conductivity of fluids with nanoparticles. *ASME-Publications-Federation* 231:99–106.
- Commission Regulation (EU) No 1253/2014. 2014. Implementing Directive 2009/125/EC of the European Parliament and of the Council with regard to Ecodesign requirements for ventilation units.
- Emerson, W. H. 1984. Making the most of run-around coil systems. *Journal of Heat Recovery Systems* 4 (4):265–70. DOI: [10.1016/0198-7593\(84\)90065-1](https://doi.org/10.1016/0198-7593(84)90065-1).
- Filipsson, P., A. Trüschel, J. Gräslund, and J. O. Dalenbäck. 2017. A thermal model of an active chilled beam. *Energy and Buildings* 149:83–90. DOI: [10.1016/j.enbuild.2017.05.032](https://doi.org/10.1016/j.enbuild.2017.05.032).
- Filipsson, P., A. Trüschel, J. Gräslund, and J. O. Dalenbäck. 2020. Performance evaluation of a direct ground-coupled self-regulating active chilled beam system. *Energy and Buildings* 209:109691. DOI: [10.1016/j.enbuild.2019.109691](https://doi.org/10.1016/j.enbuild.2019.109691).
- FläktGroup Econet Premium Installation and Maintenance Manual 2024. <https://www.flaktgroup.com/api/v1/Documents/836d971a-1706-43ea-9b62-2356438d2097?analytics=0>
- Ghiassiaan, S. M. 2018. *Convective Heat and Mass Transfer*. 2nd ed. Cambridge: Cambridge University Press.
- Holmberg, R. B. 1975. Heat transfer in liquid-coupled indirect heat exchanger systems. *Journal of Heat Transfer* 97 (4):499–503. DOI: [10.1115/1.3450418](https://doi.org/10.1115/1.3450418).
- Holmberg, R., and O. Strindehag. 1981. Vätskekopplade värmeåtervinningssystem. *VVS-Special* 1 (1):21–8.
- Jakobsen, A., B. D. Rasmussen, and S. E. Andersen. 1999. CoolPack—Simulation tools for refrigeration systems. *Scan Ref* 28 (4):7–10.
- Janssen, L. 2016. Selecting the Proper Glycol Concentration for Closed-Loop HVAC Systems. R. L. Deppmann News and Information. <https://www.deppmann.com/blog/service-tip-of-the-month/selecting-proper-concentration-glycol/>
- Johnson, A. B., R. W. Besant, and G. J. Schoenau. 1995. Design of Multi-Coil Run-Around Heat Exchanger Systems for Ventilation Air Heating and Cooling. *ASHRAE Trans* 101 (Pt. 2):967–78.
- Kays, W. M., and A. L. London. 1984. Compact heat exchangers.
- Liu, S., and M. Sakr. 2013. A comprehensive review on passive heat transfer enhancements in pipe exchangers. *Renewable and Sustainable Energy Reviews* 19:64–81. 81. DOI: [10.1016/j.rser.2012.11.021](https://doi.org/10.1016/j.rser.2012.11.021).
- London, A. L., and W. M. Kays. 1951. The liquid-coupled indirect-transfer regenerator for gas-turbine plants. *Journal of Fluids Engineering* 73 (5):529–40. DOI: [10.1115/1.4016310](https://doi.org/10.1115/1.4016310).
- Mahmoud, M., P. Filipsson, S. Brunninge, and J. O. Dalenbäck. 2022. Flow rate optimization in run-around heat recovery systems. *Applied Thermal Engineering* 200:117599. DOI: [10.1016/j.applthermaleng.2021.117599](https://doi.org/10.1016/j.applthermaleng.2021.117599).
- Mardiana-Idayu, A., and S. B. Riffat. 2012. Review on heat recovery technologies for building applications. *Renewable and Sustainable Energy Reviews* 16 (2):1241–55. DOI: [10.1016/j.rser.2011.09.026](https://doi.org/10.1016/j.rser.2011.09.026).
- MathWorks, I. 2022. MATLAB (Version R2022b) [Computer software]. <https://www.mathworks.com/>
- Nelson, G. 2021. Optimizing coil loop energy recovery systems. *ASHRAE Journal* 63 (11):10–12,14,16–18,20.

- Rabehl, R. J., J. W. Mitchell, and W. A. Beckman. 1999. Parameter estimation and the use of catalog data in modeling heat exchangers and coils. *HVAC&R Research* 5 (1):3–17. DOI: 10.1080/10789669.1999.10391220.
- Rasouli, M., S. Akbari, H. Hemingson, R. W. Besant, and C. J. Simonson. 2011. Application of a run-around membrane energy exchanger in an office building HVAC system. *ASHRAE Transactions* 117 (2):686–703.
- Robatherm 2024. Run around coils heat recovery systems for high efficient heat recovery. https://www.robatherm.com/de/system/files/robatherm_H-KVS_eng.pdf
- Trox X-CUBE 2024. Run around coil system for efficient heat recovery. https://cdn.trox.de/6dcfd3925890e0db/057a4752c022/SF_2021_08_KVS_DE_en.pdf
- Wallin, J., H. Madani, and J. Claesson. 2009. Ventilation heat recovery with run around coil - System analysis and a study on efficiency improvement - Part I. In *Ashrae RAL Symposium on Sustainability and Green Buildings*.
- Zeng, Y. Y., R. W. Besant, and K. S. Rezkallah. 1992. The effect of temperature dependent properties on the performance of run-around heat recovery systems using aqueous-glycol coupling fluids. *ASHRAE Trans* 98 (1):551–62.

Appendix A

	Exhaust air flow rate [l/s]	Supply air flow rate [l/s]	Liquid flow rate [l/s]	Outdoor air temperature [°C]	Supply air temperature [°C]	Extract air temperature [°C]	Warm liquid temperature (post pump) [°C]	Cool liquid temperature [°C]	Warm liquid temperature (pre pump) [°C]	Exhaust air temperature [°C]	Heat imbalance [%]
1	999.7	999.8	0.524	2.10	13.40	18.91	14.23	7.90	13.77	8.32	0.9
2	999.9	1000.0	0.495	2.21	13.81	19.26	14.64	7.85	14.21	8.29	1.2
3	1000.3	1000.0	0.466	2.23	14.24	19.85	15.21	7.80	15.00	8.36	3.5
4	1000.1	999.7	0.438	2.33	14.44	19.93	15.50	7.50	15.20	8.29	2.1
5	1000.3	999.9	0.410	2.23	14.22	19.59	15.40	7.00	15.20	7.89	1.9
6	1000.0	1000.0	0.382	2.32	14.64	19.86	16.09	6.64	15.84	7.84	1.5
7	1000.3	1000.0	0.353	2.32	14.85	20.14	16.63	6.40	16.32	7.79	0.3
8	999.9	999.8	0.325	2.30	14.75	19.96	16.99	5.90	16.60	7.53	-1.4
9	999.9	999.8	0.298	2.33	14.77	19.96	17.30	5.17	17.10	7.39	-0.9
10	1000.0	999.9	0.270	2.29	14.74	19.86	18.08	4.71	17.60	7.42	-1.6
11	1000.0	1000.1	0.244	2.18	14.44	19.76	18.44	4.02	18.10	7.59	0.3
12	1000.1	1000.0	0.216	2.43	13.99	19.46	18.90	3.50	18.60	8.09	1.6
13	999.7	999.8	0.190	2.45	13.11	19.30	19.20	3.22	18.91	8.69	0.9
14	999.9	999.9	0.150	2.60	11.83	19.16	19.75	2.80	19.60	10.25	5.1
15	999.6	1000.1	0.130	2.60	10.94	19.16	20.13	2.80	19.90	11.19	6.0
16	1000.0	1000.0	0.111	2.80	9.95	19.16	20.46	3.00	20.10	12.76	11.5
17	1000.2	1000.0	0.088	2.98	8.58	19.16	20.50	3.00	20.19	14.29	14.4
18	999.7	1000.1	0.068	3.03	7.54	19.06	20.50	3.00	20.10	15.57	23.7
19	749.9	749.9	0.526	3.69	14.03	19.91	14.72	10.23	14.35	10.29	0.7
20	750.0	750.0	0.499	3.72	13.99	19.70	14.65	10.14	14.20	9.97	-2.5
21	750.0	750.0	0.469	3.71	14.14	19.81	14.80	9.85	14.55	9.94	2.2
22	750.1	750.0	0.440	3.74	14.37	19.89	15.10	9.75	14.70	9.84	0.0
23	749.8	750.2	0.412	3.92	14.59	20.03	15.43	9.60	14.96	9.69	-2.9
24	750.0	749.9	0.384	3.82	14.84	20.30	15.70	9.35	15.45	9.56	0.5
25	750.1	749.9	0.355	3.91	14.94	20.29	15.95	8.97	15.47	9.28	-4.8
26	750.0	750.1	0.327	3.86	15.21	20.33	16.37	8.55	16.07	9.03	-1.7
27	749.9	750.2	0.300	3.85	15.87	20.98	17.18	8.31	16.91	8.98	-1.0
28	750.2	750.1	0.274	4.70	16.20	20.96	17.87	8.40	17.53	9.49	-1.7
29	750.0	749.8	0.247	4.80	16.14	20.56	18.13	7.86	17.86	9.02	-3.0
30	750.0	749.9	0.217	4.02	15.94	20.41	18.61	6.50	18.30	8.45	-1.4
31	750.1	749.9	0.191	4.02	15.59	20.37	19.24	5.74	19.00	8.60	-1.9
32	750.0	750.0	0.149	4.16	14.84	20.26	19.90	5.16	19.66	9.39	-1.5
33	749.9	750.1	0.130	4.32	13.94	20.14	20.35	4.85	20.13	10.34	-1.1
34	750.1	750.2	0.111	5.18	13.14	20.06	20.60	5.50	20.46	12.09	1.3
35	749.9	750.2	0.088	5.28	11.48	19.70	20.40	5.50	20.30	13.58	3.4
36	750.0	750.2	0.069	5.40	10.32	19.30	20.19	5.79	19.75	14.60	4.9
37	499.7	499.8	0.527	3.20	13.14	19.36	13.70	10.80	13.20	10.69	-2.7
38	500.2	500.1	0.497	3.20	13.14	19.43	13.70	10.60	13.20	10.49	-4.4
39	500.0	500.1	0.468	3.14	13.21	19.52	13.70	10.32	13.50	10.49	6.2
40	500.1	500.0	0.439	3.18	13.34	19.67	14.00	10.30	13.52	10.19	-5.0
41	499.8	500.1	0.410	3.21	13.54	19.86	14.20	10.20	13.70	10.18	-4.8

(Continued)

Appendix A (Continued).

	Exhaust air flow rate [l/s]	Supply air flow rate [l/s]	Liquid flow rate [l/s]	Outdoor air temperature [°C]	Supply air temperature [°C]	Extract air temperature [°C]	Warm liquid temperature (post pump) [°C]	Cool liquid temperature [°C]	Warm liquid temperature (pre pump) [°C]	Exhaust air temperature [°C]	Heat imbalance [%]
42	500.1	499.8	0.382	3.35	13.80	20.06	14.50	10.13	14.11	9.99	-3.8
43	500.0	500.1	0.354	3.36	13.84	20.06	14.43	9.80	14.20	9.99	1.0
44	500.0	500.2	0.326	3.50	14.04	20.06	14.70	9.80	14.40	9.69	-2.5
45	500.2	500.0	0.299	3.50	14.24	20.06	14.90	9.40	14.70	9.49	-0.2
46	500.1	500.1	0.272	3.53	14.63	20.16	15.50	9.10	15.10	9.19	-3.4
47	500.3	499.9	0.244	3.50	14.93	20.26	15.90	8.61	15.60	8.99	-1.1
48	500.2	500.0	0.218	3.51	15.14	20.36	16.40	8.10	16.10	8.49	-4.1
49	499.8	500.4	0.192	3.60	15.71	20.46	17.20	7.30	17.02	8.20	-1.4
50	500.0	500.1	0.169	3.60	15.94	20.65	17.80	7.00	17.59	8.08	-2.2
51	499.8	499.9	0.150	3.64	16.14	20.76	18.80	6.27	18.40	7.89	-4.6
52	499.7	500.0	0.140	3.70	15.91	20.55	18.80	5.99	18.40	8.04	-4.0
53	500.1	499.8	0.130	3.70	15.44	20.01	18.80	5.41	18.40	8.00	-3.7
54	499.9	500.1	0.111	3.75	14.74	19.81	19.15	4.99	18.94	8.49	-2.7
55	500.2	500.0	0.088	3.80	13.45	20.16	20.40	4.40	20.28	10.36	-0.1
56	499.7	500.0	0.069	4.05	11.64	20.16	20.60	4.40	20.60	12.21	-1.7
57	250.3	249.9	0.520	2.70	12.64	19.56	13.10	11.39	12.81	11.19	-2.0
58	250.1	250.1	0.491	2.70	12.67	19.66	13.30	11.30	12.90	11.19	-8.8
59	249.6	250.0	0.460	2.70	12.74	19.76	13.30	11.30	12.90	11.00	-9.2
60	249.8	250.1	0.432	2.70	12.74	19.76	13.30	11.22	12.90	10.99	-7.8
61	249.7	250.3	0.404	2.70	12.79	19.86	13.30	11.10	12.90	10.99	-6.6
62	250.3	250.1	0.376	2.70	12.84	19.86	13.30	11.05	12.90	10.80	-6.8
63	250.6	249.7	0.349	2.62	12.84	19.86	13.30	10.80	12.90	10.65	-6.2
64	250.0	250.1	0.321	2.60	12.84	19.96	13.30	10.60	12.95	10.49	-4.7
65	250.1	249.9	0.293	2.60	12.86	19.96	13.56	10.47	13.10	10.34	-8.8
66	250.2	250.2	0.266	2.60	12.87	19.84	13.33	10.18	13.18	9.99	1.3
67	249.7	250.2	0.240	2.60	13.08	19.85	13.62	9.90	13.25	9.76	-5.0
68	249.6	250.0	0.213	2.60	13.34	20.00	14.10	9.70	13.70	9.49	-5.9
69	249.7	249.8	0.186	2.60	13.65	20.10	14.38	9.23	14.00	9.19	-5.0
70	249.9	249.9	0.149	2.60	14.24	20.26	15.22	8.50	14.80	8.61	-5.1
71	249.8	250.1	0.130	2.60	14.64	20.36	15.80	7.86	15.50	8.28	-2.5
72	250.1	249.6	0.118	2.60	14.98	20.26	16.22	7.30	15.80	7.81	-4.4
73	249.4	250.4	0.110	2.40	15.14	20.16	16.42	6.81	16.01	7.55	-1.6
74	250.0	250.4	0.103	2.40	15.14	20.06	16.70	6.35	16.50	7.32	-0.3
75	250.1	249.5	0.095	2.40	15.14	20.06	17.20	6.10	17.00	7.29	-0.8
76	250.2	249.9	0.088	2.40	15.14	20.10	17.70	5.50	17.30	7.21	-3.3
77	250.3	250.1	0.081	2.60	15.13	20.16	18.50	4.80	18.10	7.39	-3.7
78	250.4	249.9	0.068	2.60	14.56	19.96	18.86	4.30	18.60	7.79	-2.0
79	250.2	249.9	0.060	2.53	13.84	19.96	19.30	3.77	19.10	8.29	-2.7
80	249.9	250.3	0.053	2.60	13.04	19.96	19.80	3.50	19.60	9.19	-2.0
81	250.0	250.2	0.041	2.60	11.38	19.96	20.10	2.97	19.80	10.83	-2.8
82	250.4	249.6	0.030	2.41	8.97	19.86	20.25	2.70	20.00	12.91	-4.0